Simulations and Experiments of Etching of Silicon in HBr Plasmas for High Aspect Ratio Features

Helen H. Hwang[a)] and M. Meyyappan
NASA Ames Research Center
Moffett Field, CA 94035 USA

G. S. Mathad and R. Ranade
Infinion Technologies, Inc.
Hopewell Junction, NY 12533 USA

Abstract

Etching in semiconductor processing typically involves using halides because of the relatively fast rates. Bromine containing plasmas can generate high aspect ratio trenches, desirable for DRAM and MEMS applications, with relatively straight sidewalls. We present scanning electron microscope images for silicon-etched trenches in a HBr plasma. Using a feature profile simulation, we show that the removal yield parameter, or number of neutrals removed per incident ion due to all processes (sputtering, spontaneous desorption, etc.), dictates the profile shape. We find that the profile becomes pinched off when the removal yield is a constant, with a maximum aspect ratio (AR) of about 5 to 1 (depth to height). When the removal yield decreases with increasing ion angle, the etch rate increases at the corners and the trench bottom broadens. The profiles have ARs of over 9:1 for yields that vary with ion angle. To match the experimentally observed etched time of 250 s for an AR of 9:1 with a trench width of 0.135 μm, we find that the neutral flux must be 3.336×10^{17} cm^2 s^{-1}.

[a)] Electronic mail: hwang@dm1.arc.nasa.gov

I. Introduction

Etching of silicon in the semiconductor industry is typically accomplished using halide-containing plasmas, such as chlorine, fluorine, and bromine. Anisotropic profiles can be etched with ion-assisted etching using chlorine plasmas with fairly rapid etch rates. There are many advantages of using a relatively mature technology such as chlorine-based chemistry, such as fast etch rates, as well as having well-characterized material quantities and behavior (sputter yields,[1] removal yields,[2] etc.). However, there are disadvantages to chlorine, such as poor selectivity to photoresist, as well as difficulty achieving high aspect ratio (AR) features. Other chemistries, such as bromine containing plasmas, have been demonstrated to etch highly anisotropic profiles[3,4] and are frequently used in commercial systems. Certain applications require extremely high AR devices, such as etching via holes, DRAM, and MEMS fabrication, which means that using solely chlorine-based chemistry is not viable.

In bromine systems, the chemical mechanism of thermal etching has been studied,[5,6] as well as recombination on the surface.[7] In spite of the fact that bromine has been used for more than fifteen years, its etch mechanism is not well understood and obtaining material properties, such as etch yields as a function of incident ion angle and sticking coefficients of Br and Br_2, is difficult. In general, bromine ion-assisted etch rates are seen to be lower than that for chlorine by a factor of about 1.6.[8] Although bromine etch yields are higher than for chlorine, it is thought that bromine adsorption onto the silicon surface has a considerably higher activation energy, which leads to a lower overall etch rate for bromine.[9] The total sputter yield for Br^+ has been measured to be higher than that for Cl^+, although the chemical sputter yield for Cl^+ is higher.[10]

In this article, we will describe the simulation we used to calculate etched silicon trenches in bromine containing plasmas. We will show experimentally obtained high aspect ratio Si

trenches that were etched in HBr plasmas. We will show results from a feature profile evolution simulation that demonstrates the effect of ion removal yields on profile tapering and maximum obtainable AR. The yield magnitudes, as well as the functional dependence on ion impact angle, determine the width of the trench bottom. We will also make comparisons to the experimentally obtained SEMs.

II. Experimental conditions

The trenches are etched in Si with HBr plasma generated in a magnetically enhanced, capacitively coupled reactor with an applied frequency of 13.56 MHz. The inter-electrode gap is 27 mm. The upper electrode has a quartz showerhead gas distribution plate to facilitate a uniform distribution of etching gases over the 200 mm diameter wafer. In addition, the reactor wall is outfitted with a quartz cylindrical shield for easy cleaning. The reactor itself is made of anodized aluminum. The reactor metal walls, as well as upper and lower electrodes, are at 60° C during processing. The wafer, however, reaches a different temperature depending on the process conditions, particularly RF power and reactor pressure. The cathode, or the lower electrode, also has a quartz focus ring 6 mm high, surrounding the wafer. The ring serves to reduce the electric field at the edge, resulting in improved etch uniformity. The wafer is held to the cathode by electrostatic force, the cathode being an electrostatic chuck with polyimide dielectric coating applied to the top surface of the cathode. An independent DC voltage is applied to the lower electrode to produce the desired electrostatic force. A magnetic field of 170 Gauss is applied by a set of rotating magnets, which facilitates a uniform field. The process conditions are 1300 W, 75 mTorr, and 175 sccm HBr. An SEM sample of the etched trenches is shown in

Fig. 1, with a mask bevel of ±75°. The trenches are etched with high ARs of approximately 9:1, although the trenches taper at the bottom. The width at the bottom of the trench is roughly half of the width at the opening (surface), which is 0.135 μm wide. A close-up view of the trenches is provided in Fig. 2. The bottom of the trench is curved, which indicates that neutral shadowing decreases etching in the corners. This curvature suggests that the high AR of the trench limits the neutral flux at the bottom and lowers the neutral to ion flux ratio arriving from the plasma ($\Gamma_n/\Gamma_+ \sim 1$). Also, since the trench is tapered, the ions are strongly directed toward the substrate with an anisotropic distribution function. The actual etch time was 4 minutes 10 sec (250 seconds).

III. Etch rate calculation

Here we provide a brief summary of the approach we use to calculate trench etching. To describe the etch process, we assume a two step mechanism for etching of Si in HBr, similar to Cl etching of Si. This methodology is similar to that described earlier,[11] except here we distinguish between the two neutral species, Br and Br_2. Passivation of silicon occurs due to Br and Br_2 reacting with Si to form $SiBr_x$. Positive ions (HBr^+, Br^+) impact the brominated surface and etching proceeds due to formation of volatile products. As in most commercial systems, obtaining plasma diagnostics was impossible due to reactor limitations; therefore, a simulation of the plasma conditions would lend few insights as there were too many unknowns to estimate and compare (species fluxes, electric fields, etc.). Instead, the species fluxes were calculated by estimating the distribution functions for the ions and neutrals. The distribution function for the neutrals was assumed to be Maxwellian. The ions were assumed to be Maxwellian in the bulk plasma and to fall collisionlessly through a sheath with voltage V_s. Based on the tapered profiles

obtained in Figs. 1 and 2, the distribution functions for the ions have been selected to be strongly anisotropic and have the same analytic form given in Ref. 11, with $eV_s/kT_i = 100$.

Using these estimated distribution functions, the fluxes must be calculated at each point in the 2-D (x, y) computational domain around the trench. The directed velocity (of either ion or neutral) has the form $|v|\cos(\theta - \xi)$, where $|v|$ is the magnitude of the total velocity, θ is the impacting angle from the normal, and ξ is the angle of the surface from the normal. The impacting angle is defined as

$$\theta = \tan^{-1}\left(\frac{v_x}{v_y}\right). \tag{1}$$

Then the directed flux from the plasma to a point on the surface is

$$\Gamma_{\text{plasma}} = \int_{\theta_1}^{\theta_2}\int_{0}^{v_{\max}} |v|\cos(\theta - \psi)\cdot f(|v|,\theta)\cdot|v|\, d|v|\, d\theta\,. \tag{2}$$

Note that Eq. 2 does not include re-emission fluxes from the trench surface. Both ion and neutral fluxes are calculated according to Eq. 2 for each species. The net ion flux is summed over all ion species and the neutral flux is calculated from the sum of the fluxes of Br and Br_2. Re-emission fluxes for neutrals are neglected by setting the sticking coefficients equal to unity. This approximation represents the maximum possible etch rate by assuming that all neutrals will react with the surface. Ion re-emission fluxes are ignored, as microtrenching is generally not seen in trenches etched in HBr plasmas compared to chlorine plasmas.[12]

In order to consider two separate neutral species, surface coverage parameters for both Br and Br_2 must be calculated. Experimental evidence has shown that bromine etch, like chlorine,

can be considered to occur in a monolayer,[4,13] hence using a surface site balance model is a valid assumption:

$$\sigma_{Br}\frac{\partial\alpha_{Br}}{\partial t}=\Gamma_{Br}S_{Br}\left(1-\alpha_{Br}-\alpha_{Br_2}\right)-\Gamma_{+}Y_{Br}\alpha_{Br} \tag{3}$$

$$\sigma_{Br_2}\frac{\partial\alpha_{Br_2}}{\partial t}=\Gamma_{Br_2}S_{Br_2}\left(1-\alpha_{Br}-\alpha_{Br_2}\right)-\Gamma_{+}Y_{Br_2}\alpha_{Br_2} \tag{4}$$

Here, α is the surface coverage, σ is the areal density, S is the sticking coefficient, Γ_+ is the total ion flux, and Y is the removal yield, or number of atoms or molecules removed per incident ion. Note that the removal yield can be due to sputtering, spontaneous emission, etc. The surface coverages are found by assuming steady state and thus setting $\partial\alpha/\partial t = 0$. Each surface coverage parameter is then a function of removal yields and ion and neutral fluxes. Let

$$D=\Gamma_{Br}S_{Br}\Gamma_{+}Y_{Br_2}+\Gamma_{Br_2}S_{Br_2}\Gamma_{+}Y_{Br}+\left(\Gamma_{+}\right)^2Y_{Br}Y_{Br_2}. \tag{5}$$

Then the surface coverages for Br and Br_2 are

$$\alpha_{Br}=\frac{\Gamma_{Br}S_{Br}\Gamma_{+}Y_{Br_2}}{D}, \tag{6}$$

$$\alpha_{Br_2}=\frac{\Gamma_{Br_2}S_{Br_2}\Gamma_{+}Y_{Br}}{D}. \tag{7}$$

Assuming that the etch yield of silicon (Y_{Si}) is the same for all impacting ions, then the resulting etch rate is

$$ER = \frac{1}{\rho_{Si}} \cdot \sum_{ions} \left(\alpha_{Br} + \alpha_{Br_2}\right) Y_{Si} \Gamma_+ , \tag{8}$$

where ρ_{Si} is the mass density of silicon. The etch yield is dependent on impacting ion angle and has the functional form given in Ref. 1.

Note that the properties that determine the uniqueness of a neutral species are its sticking coefficient, removal yield, and mass (which determine the distribution function). If $S_{Br} = S_{Br2}$ and $Y_{Br} = Y_{Br2}$, then Br and Br_2 are considered to be indistinguishable, etch wise. Furthermore, equations 6 and 7 then collapse to form the expressions for α and *ER* given in Ref. 11 for one effective neutral species (denoted *n*),

$$\alpha = \frac{S_n \Gamma_n}{S_n \Gamma_n + Y_{Br} \Gamma_+} \tag{9}$$

with an etch rate given by

$$ER = \frac{1}{\rho_{Si}} \cdot Y_{Si} \cdot \Gamma_+ \cdot \alpha . \tag{10}$$

IV. Simulation of Profile Evolution using Level Sets (SPELS)

We have developed a feature profile evolution simulation, SPELS, which has been described earlier.[11] The level set equation is used to advance a higher order variable $G(x, y, t)$, in which the plasma-surface interface occurs at $G(x, y, t_0) = 0$, or the zero level set. The plasma is defined where $G(x, y, t) > 0$ and the substrate by $G(x, y, t) < 0$. On the interface, the etch rate is

equal to the negative of the speed (S) of G. In the remaining (x, y) domain, G is updated by solving the level set equation,

$$\frac{dG}{dt} + S|\nabla G| = 0. \tag{10}$$

Therefore, the trench movement is indirectly tracked as G is advanced. The simulation continues for a user-specified time.

It has been found that to obtain good resolution of the evolving feature, the mesh resolution typically requires about 80 × 80 cells per 1 × 1 normalized *X/L*, *Y/L* area. This would mean having 880 × 160 cells to model ARs of 9:1. Calculating the flux integrals over the entire mesh is computationally expensive and slows down the code significantly when the mesh is large. In order to run the simulation in a reasonable time, a narrow banding technique has been implemented. This technique is based upon the method derived by Adalsteinsson and Sethian[14] and is outlined below. The level set equation is solved only in a "band" around the zero level set, thus reducing the number of "active" cells. G is set to a minimum (negative) value beyond the edge of the band in the solid, and a maximum value in the plasma above the band edge, as shown in Fig. 3. The band is reconstructed whenever the zero level set gets close to the edge of the band. For the following cases, the band is approximately 22 cells wide (11 cells above and below the zero level set), and the band is reconstructed whenever the zero level set gets within 6 cells of the edge of the band. Using this method, the computational speed-up is a factor of 5 or more.

Obtaining most physical quantities for Br etching of silicon is difficult, as many of the parameters are unknown for HBr interactions with Si. As a first attempt, we have assumed

material parameters that are similar to chlorine, given in Ref. 11, unless specified otherwise. We also assume that the form of the silicon etch yield versus ion impact angle for Br and Br_2 is similar to that of chlorine given in Ref. 1, although calculations involving the relative etch yield for HBr is considered later in this article. In the following cases, we do not consider diffusive re-emission of neutrals and instead set the sticking coefficients of Br and Br_2 to unity. The normalized length scale is $L = 0.135$ μm. The amount of recombination of bromine on the reactor surfaces is unknown and we assume that the ratio of neutral fluxes from the plasma $\Gamma_{Br2} / \Gamma_{Br} = 3$ and the ratio of the ion fluxes is $\Gamma_{Br+} / \Gamma_{HBr+} = 3$. The ratio of the total neutral flux to the total ion flux is unity ($\Gamma_n / \Gamma_+ = 1$). The hard mask is assumed to be a height of $0.2\ L$, which corresponds to about ±78° angle allowance at the center of the trench, which is similar to the experimental mask bevel allowance.

V. Results and Discussion

The following results were obtained using the formulation given in Eqs. 6-8 for the surface coverages and etch rates. In Fig. 4(a), $Y_{Br} = Y_{Br2} = 1$ (meaning Br and Br_2 have identical properties), leading to a maximum aspect ratio of 5:1 for the trench. The neutrals become shadowed inside the trench and are less able to brominate the surface, particularly in the corners. The etch rate subsequently slows down at the corners and the trench pinches off. Increasing the removal yields to $Y_{Br} = Y_{Br2} = 3$, as shown in Fig. 4(b), broadens the trench slightly but the maximum AR is still not substantially greater than 5:1.

The trenches shown in Fig. 4 assume that the removal yields Y_{Br} and Y_{Br2} are constant with impacting ion angle. This assumption may not be correct, as the removal yield encompasses

all methods of removing the brominated surface species, including physical sputtering. For example, ion assisted etch yields have been shown to be a strong function of ion angle (Ref. 1), and are included in calculating $Y \cdot \Gamma_+$. The trenches shown in Fig. 5 employ Y_{Br} and Y_{Br2} which vary with impacting ion angle in the same way that Y_{Si} varies. In Fig. 5(a), the maximum removal yield $Y_{Br} = Y_{Br2} = 1$, and in Fig. 5(b), the maximum yield is $Y_{Br} = Y_{Br2} = 3$, corresponding to cases in Figs. 4(a) and (b), respectively. In these cases, using a yield that varies with ion angle leads to increased surface coverages in the corners. The higher surface coverages create broader trenches and thus generate higher aspect ratios. The trench in Fig. 5(a) is more square than the pinched off trench in Fig. 4(a), although there is some bowing of the sidewalls. Increasing the removal yield in Fig. 5(b) leads to a flared trench, which has a severe amount of undercutting. Both trenches have rounded bottoms, which indicates that the surface coverages vary along the bottom due to neutral shadowing. Higher aspect ratios will increase the amount of shadowing.

Allowing an angular dependent removal yield essentially scales the total ion flux and modifies the surface coverages in the following way. Both α_{Br} and α_{Br2} can be calculated using Eqs. 6 and 7, but instead have the following expression instead of Eq. 5:

$$D = \Gamma_{Br} S_{Br} \Gamma_+ Y_{Br_2} + \Gamma_{Br_2} S_{Br_2} \Gamma_+ Y_{Br} + \beta (\Gamma_+)^2 Y_{Br} Y_{Br_2}, \tag{11}$$

where $0 \le \beta \le 1$. Hence surface coverages that depend on ion angle will always be equal to or larger than the coverages using constant removal yields. The amount of "flare" in the trench can be dictated by varying the dependency of Y_{Br} and Y_{Br2} on ion angle. For example, one can select an artificially strong dependence on ion angle such as

$$Y_n = Y_0 \exp(-|\theta - \xi|). \tag{12}$$

This extreme dependence leads to undercutting as shown in Fig. 6. Allowing the removal yields of both Br and Br_2 to vary according to Eq. 12 increases the surface coverages in the corners and causes severe undercutting. In contrast, the corners become shadowed and do not etch when the removal yield is set to a constant value ($Y_{Br} = Y_{Br2} = 1$). This constant value yield case is the same as shown in Fig. 4(a); these two cases represent the two extremes for the functional dependence of the removal yield on impact angle. The example shown in Fig. 6 and given in Eq. 12 is for demonstration purposes only, as the removal yield is expected to depend on ion angle in a similar fashion to the ion-enhanced sputter yield. When the removal yield is constant, the neutrals do not sufficiently brominate the corners and thus the trench pinches off, creating a low AR trench.

The following cases use a removal yield for Br and Br_2 that varies with ion impact angle. The yields given are for the maximum values, and the functional form varies in the same manner as does the etch yield Y_{Si}. Including an angular dependence of the removal yields can cause a flared shape, as seen in Figs. 5(b) and 6. However, the amount of tapering in the trench can also be adjusted by scaling the maximum value of Y_{Br}. For large removal yields ($Y_{Br} = Y_{Br2} = 3$) as seen in Fig. 7 (a), the trench is undercut much in the same way that as is the profile in Fig. 6. In other words, assuming the removal of Br and Br_2 on the surface is less preferential for ions that impact at grazing angles causes the trench to etch more in the corners and thus leads to the flared shape. The tapered trench shown in Fig. 7(b) results from a low removal yield, or $Y_{Br} = Y_{Br2} =$ 0.4, which essentially sets the ion-assisted etch yield equal to the removal yield (no spontaneous desorption of neutrals).

The above cases all assumed that both Br and Br_2 had identical sticking coefficients and removal yields. The trenches shown in Figs. 8(a) and (b) assume different removal yields for Br and Br_2. For both cases, $\Gamma_{Br2}/\Gamma_{Br} = 3$, meaning a low degree of dissociation. The trench in Fig. 8(a) has $Y_{Br} = 0.4$ and $Y_{Br2} = 3$, which leads to a flared trench as the majority of the neutral flux is Br_2 which has a high removal yield. The tapered trench in Fig. 8(b) has the opposite yields, or $Y_{Br} = 3$ and $Y_{Br2} = 0.4$. Again, the dominant neutral flux and its removal yield will dictate the shape of the trench.

Vitale *et al.*[15] measured relative etch yields for HBr and Br_2 and found that the yields have a weaker dependence on ion impact angle than does the yield for Cl_2, which was originally measured in Ref. 1. These differences are shown in Fig. 9. The etch yield for Cl is constant for small angles of incidence, but then has a sharp drop-off for large angles. In contrast, the etch yield for HBr has a slow decrease with increasing ion angle. However, it should be noted that the authors indicate that the experimental error is significant for larger angles (approximately ±53% for HBr compared to ±17% for Cl_2). The angular dependencies for etch yields for chlorine and HBr fall within each other's error ranges, making it difficult to determine if the overall shapes are correct. In any case, for high aspect ratio cases the overall angular dependency of the etch yield may not be significant in determining profile shapes. The case shown in Fig. 10(a) uses Vitale's etch yield and has the same overall profile shape as does the case in Fig. 10(b), which uses Chang's yield for chlorine. The magnitude of the etch yield in Fig. 10(a) is twice that in Fig. 10(b); however, the tapered trench shape is indicative of etching that is limited by neutral shadowing. Both cases assume that the removal yield has the same angular dependence as their respective etch yields. Because ion reflections are not considered, the profile shape is not

strongly dependent on the angular dependence of the etch yield, although the overall etch rate does increase.

Although the overall AR obtained from the model can be matched to the experimental SEMs, the profile shape differs for the bottom portion of the trench. This difference can be seen clearly in Fig. 11, where the model results from Fig. 7(b) are superimposed on the SEM. The etched trench has a gradual tapering, whereas the predicted profile is broader and suddenly tapers at the bottom. Using an ion-assisted yield of $Y_{Si} = 0.4$, the total neutral flux required to match the experimental etch time is 3.336×10^{17} cm^{-2} s^{-1}. Several possibilities exist as to why the profile shapes do not match exactly. Other phenomena, which were not considered in our simulation, may contribute to the overall profile shape. For example, it is possible that ion reflection may contribute to etching. Vyvoda et al.[16] theorized that in HBr plasmas, ions reflect off of the silicon in a diffuse distribution. Although their model overpredicted the amount of etching in the corners for a trench with AR ~ 3.3:1, they did find that their results were sensitive to the assumed reflected ion distribution. Thus, reflected ions contributing to the etch process, particularly in the corners, may account for the difference in the actual profile versus the calculated one. Other secondary processes, such as H-atom enhancement of the etch rate due to coadsorbtion,[8] lattice penetration, and Si backbond breakage,[15] may also contribute to the broader trench bottom profiles. Another possibility is that our calculation is 2-D in nature, and solving for a full 3-D calculation of the etch may improve the profile shape.

VI. Concluding Remarks

Trenches with aspect ratios of 9:1 were etched in HBr plasmas. Incorporating a narrow band technique allowed for calculations of large geometries that would otherwise not be possible.

This is particularly important for high aspect ratio etching, where trenches can exceed ARs of 20:1. For the calculated profiles, the removal yield of a neutral on silicon was found to be important for it can dictate the profile shape. Higher yields lead to broader trench bottoms (and ultimately to higher aspect ratios). If the yield has a functional dependence on ion impact angle in the same manner as the ion assisted etch yield, the trench bottom can become significantly wide and become flared. Although the overall AR can be matched to experimental values, many parameters (sticking coefficients, species fluxes, etc.) are unknown and were estimated, thus the predicted profile shapes are different. This also emphasizes the need to integrate the feature evolution model to a reactor model self-consistently in order to obtain various fluxes; however, the current limitation is the lack of knowledge on collisional cross sections for electron and ion impact reactions and details of surface chemistry.

Figure Captions

Fig. 1. SEM of etched trenches of silicon obtained in HBr plasma reactor. Aspect ratio is 9:1 per trench with etch opening of 0.135 μm. Total etched time is 250 seconds.

Fig. 2. Close-up view of trenches. Trenches have gradually tapered sidewalls and curved bottoms, which indicate neutral shadowing. Neutrals are shadowed both due to the high AR and because of low neutral flux relative to the ion flux from the plasma.

Fig. 3. Sample of contours from SPELS which define the location of the plasma-substrate interface. The narrow band technique only defines G "near" the front. (a) For plasma locations far away from the surface, $G = G_{max}$. The substrate far from the surface is defined by $G = G_{min}$. (b) A close-up view of the contours shows that within the band, $G > 0$ defines the plasma region, $G = 0$ defines the surface, and $G < 0$ indicates the substrate.

Fig. 4. Profiles generated from SPELS. Pinched off trenches with maximum AR 5:1, with constant values of removal yields. Total ratio of neutral flux to ion flux is unity. Neutrals are shadowed in the corners which prevent obtaining higher ARs. (a) $Y_{Br} = Y_{Br2} = 1$, and (b) $Y_{Br} = Y_{Br2} = 3$.

Fig. 5. Same conditions as in Fig. 4, except removal yields are functions of ion impact angle. Less removal of Br and Br_2 in the corners of the surface allow for deeper etching. (a) $Y_{Br} = Y_{Br2} = 1$, and (b) $Y_{Br} = Y_{Br2} = 3$.

Fig. 6. Difference between constant removal yield function and one that varies with ion impact angle. The dotted line is for the same case in Fig. 4(a), and the solid line has the extreme functional dependence of removal yield on ion impact angle given in Eq. 12.

Fig. 7. Tapered and flared trenches with non-constant removal yields. Both removal yields have functional forms similar to etch yield of Si with Cl, as given in Ref. 1. (a) $Y_{Br} = Y_{Br2} = 3$ and (b) $Y_{Br} = Y_{Br2} = 0.4$.

Fig. 8. Profiles assuming different removal yields for Br and Br_2. For both cases, $\Gamma_{Br2}/\Gamma_{Br} = 3$. (a) $Y_{Br} = 0.4$ and $Y_{Br2} = 3$. (b) $Y_{Br} = 3$ and $Y_{Br2} = 0.4$. The dominant neutral flux and its removal yield define the shape of the trench.

Fig. 9. Experimentally observed silicon etch yields as a function of impacting ion angle, taken from Refs. 1 and 15. The etch yield in HBr plasmas is weakly dependent on ion angle, whereas the etch yield in chlorine plasmas demonstrates a sharp decrease with large angles. Error estimates for the HBr etch yield at large angles is ±53%, and ±17% for chlorine for mid-range angles.

Fig. 10. Comparison of profiles using etch yields shown in Fig. 10. (a) Etch yield using angular dependency for HBr with $Y_{Br} = Y_{Br2} = 0.2$. (b) Etch yield using chlorine angular dependency, with $Y_{Br} = Y_{Br2} = 0.4$ (same as in Fig. 7(b)).

Fig. 11. Superimposed model results from Fig. 7(b) on the SEM from Fig. 1. The aspect ratio can be matched but the profile shapers differ, largely in part due to estimated yields as well as ion and neutral fluxes.

References

[1] J. P. Chang and H. H. Sawin, *J. Vac. Sci. Technol. A* **15**, 610 (1997).

[2] A. D. Bailey, M. C. M. van de Sanden, J. A. Gregus, and R. A. Gottscho, *J. Vac. Sci. Technol. B* **13**, 92 (1995).

[3] A. M. El-Masry, F-O. Fong, J. C. Wolfe, and J. N. Randall, *J. Vac. Sci. Technol. B* **6**, 257 (1988).

[4] T. D. Bestwick and G. S. Oehrlein, *J. Vac. Sci. Technol. B* **8**, 1696 (1990).

[5] K. Nakayama, C. M. Aldao, and J. H. Weaver, *Phys. Rev. B* **59**, 893 (1999).

[6] C. F. Hermann and J. J. Boland, *Phys. Rev. Lett.* **87**, 115503 (2001).

[7] G. P. Kota, J. W. Coburn, and D. B. Graves, *J. Vac. Sci. Technol. A* **7**, 282 (1999).

[8] C. C. Cheng, K. V. Guinn, I. P. Herman, and V. M. Donnelly, *J. Vac. Sci. Technol. A* **13**, 1970 (1995).

[9] Z. H. Walker and E. A. Ogryzlo, *J. Appl. Phys.* **69**, 2635 (1991).

[10] S. Tachi and S. Okudaira, *J. Vac. Sci. Technol. B* **4**, 459(1986).

[11] H. H. Hwang, T. R. Govindan, and M. Meyyappan, *J. Electrochem. Soc.* **146**, 1889 (1999).

[12] M. A. Vyvoda, H. Lee, M. V. Malyshev, F. P. Klemens, M. Cerullo, V. M. Donnelly, D. B. Graves, A. Kornblit, and J. T. C. Lee, *J. Vac. Sci. Technol. A* **16**, 3247 (1998).

[13] J. Pelletier and M. J. Cooke, *J. Vac. Sci. Technol. B* **7**, 59 (1989).

[14] D. Adalsteinsson and J. A. Sethian, *J. Comp. Phys.* **118**, 269 (1995).

[15] S. A. Vitale, H. Chae, and H. H. Sawin, *J. Vac. Sci. Technol. A* **19**, 2197 (2001).

[16] M. A. Vyvoda, M. Li, D. B. Graves, H. Lee, M. V. Malyshev, F. P. Klemens, J. T. C. Lee, and V. M. Donnelly, *J. Vac. Sci. Technol. B* **18**, 820 (2000).

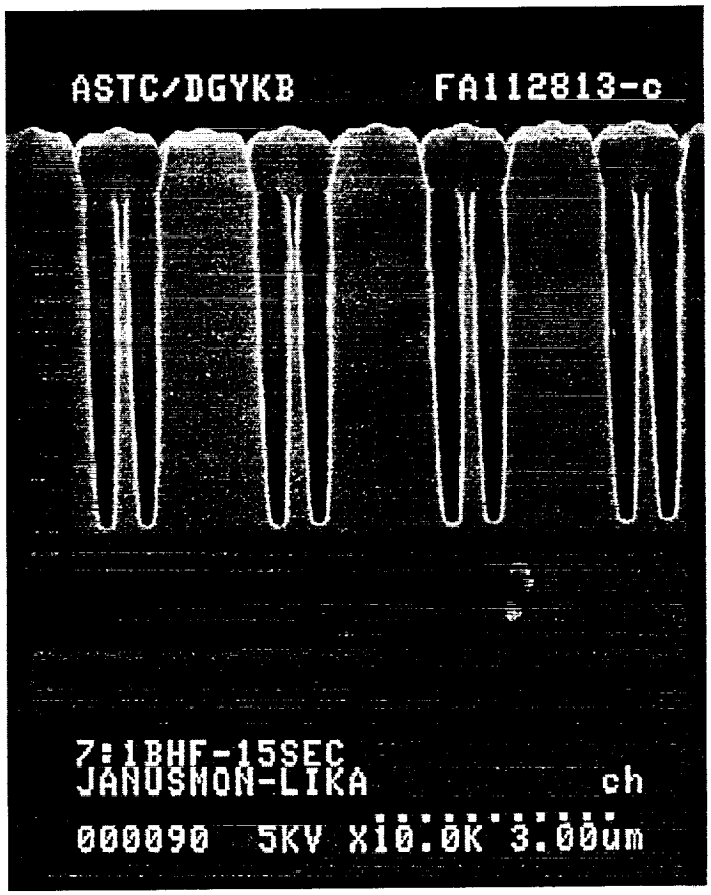

Fig. 1 of 11
Hwang et al.

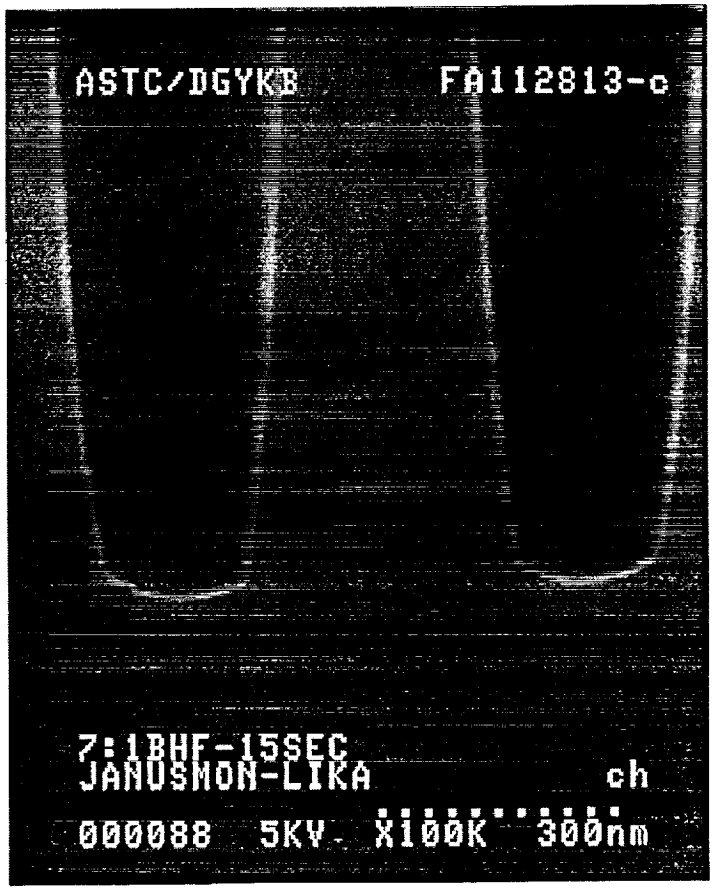

Fig. 2 of 11
Hwang et al.

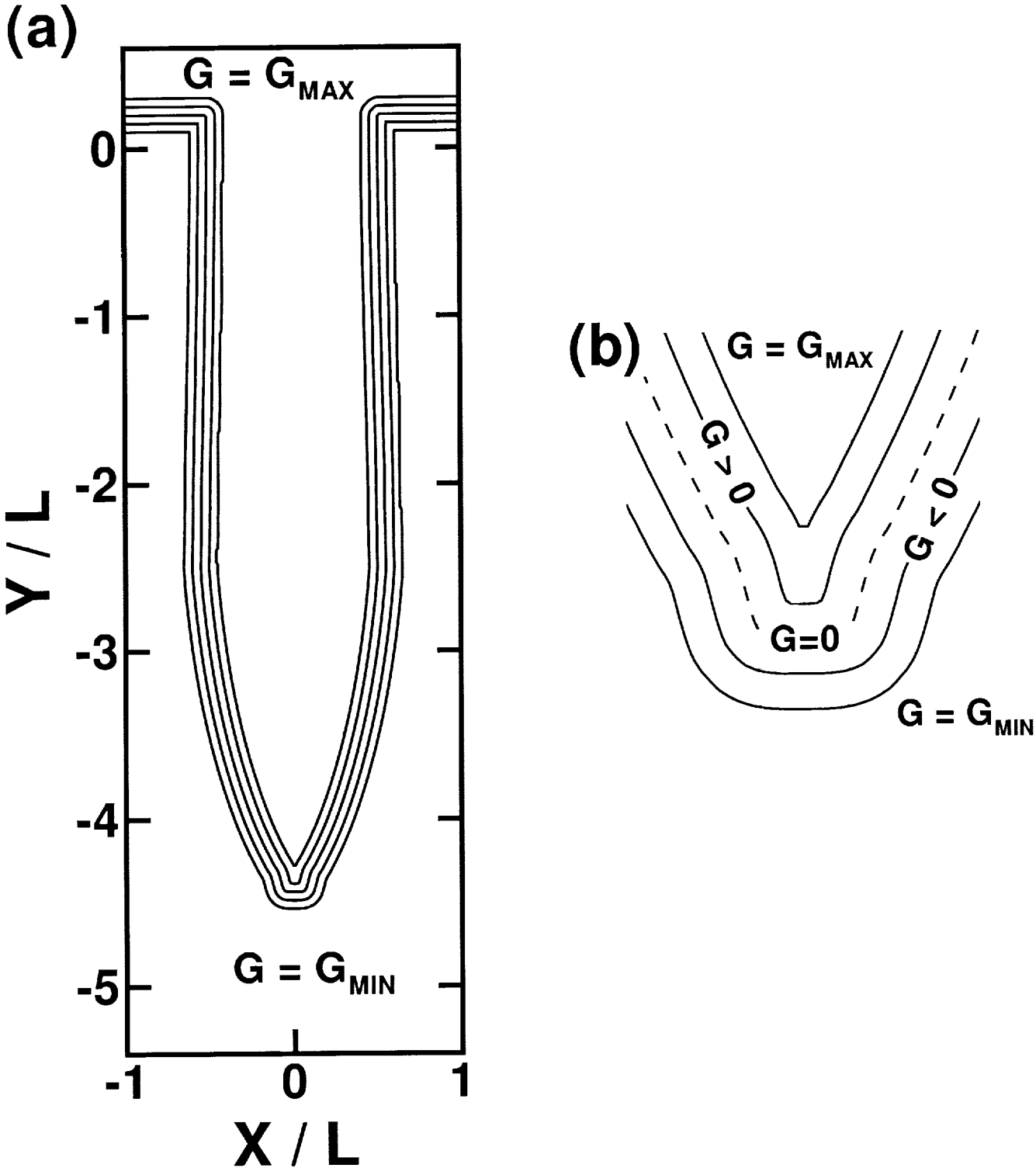

Fig. 3 of 11
Hwang et al.

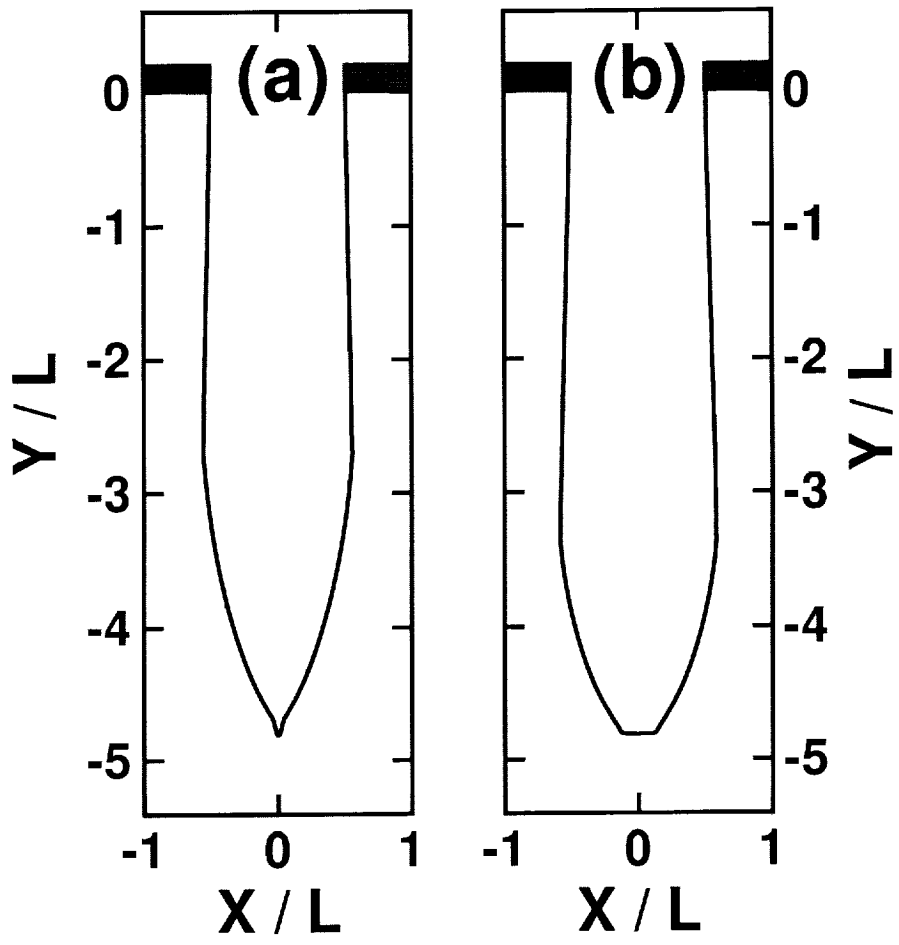

Fig. 4 of 11
Hwang et al.

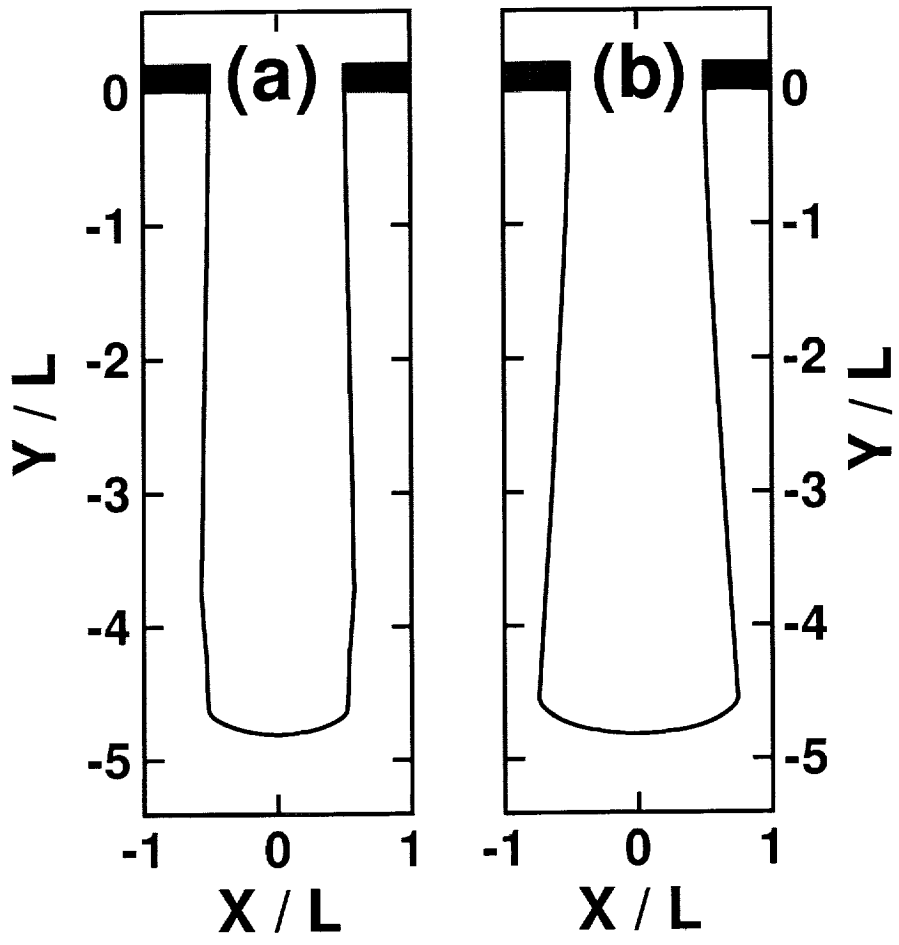

Fig. 5 of 11
Hwang et al.

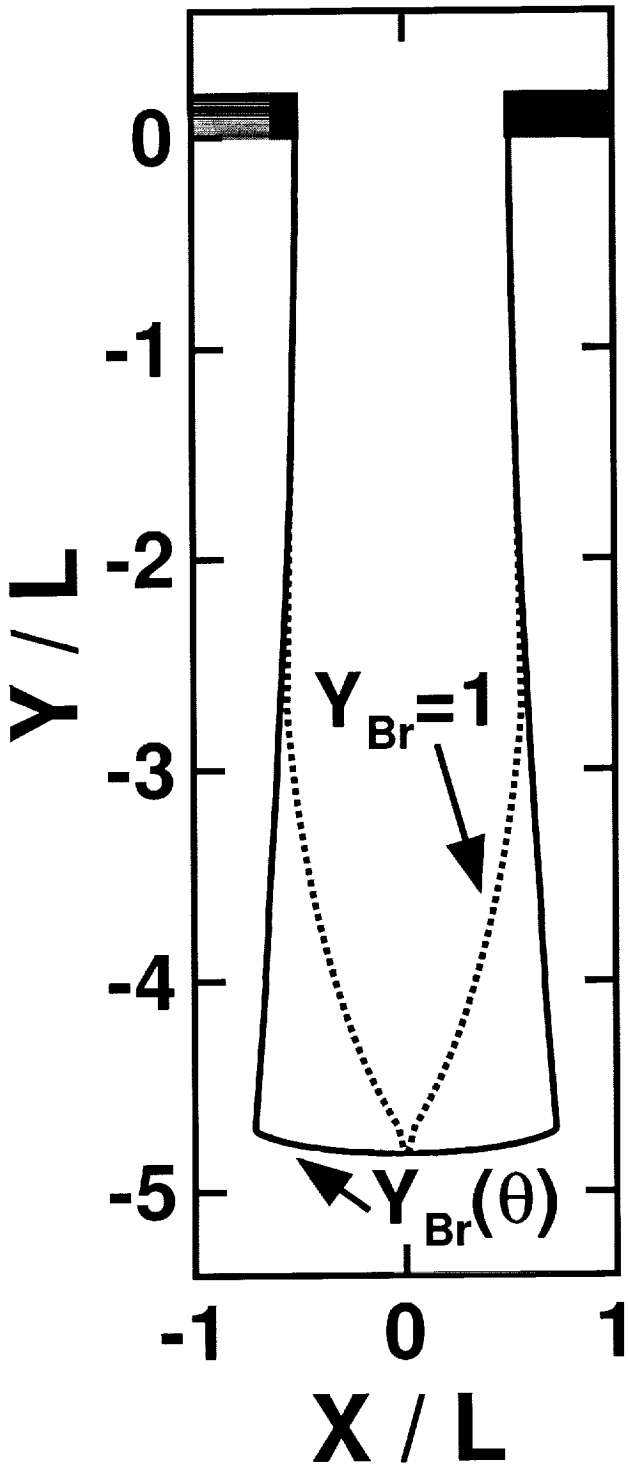

Fig. 6 of 11
Hwang et al.

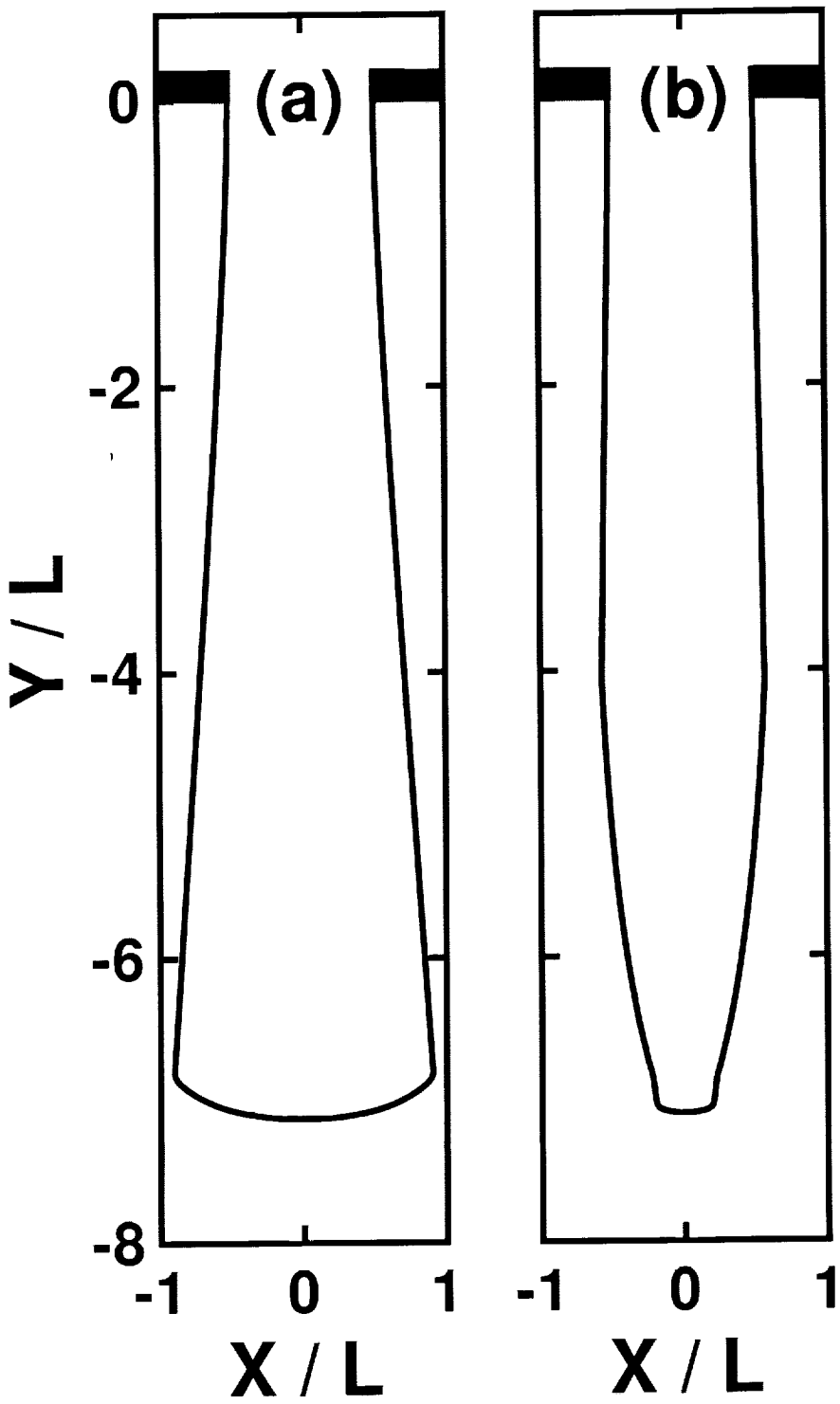

Fig. 7 of 11
Hwang et al.

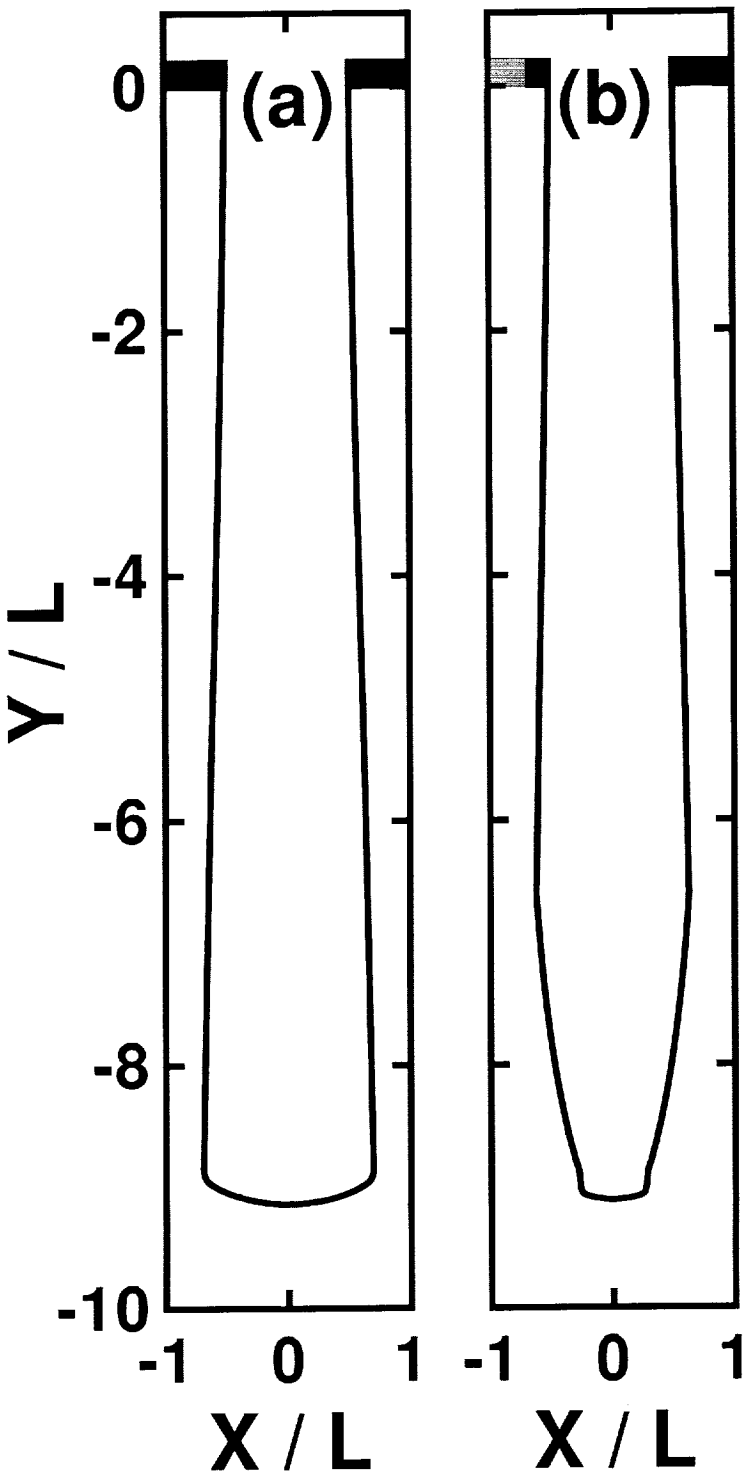

Fig. 8 of 11
Hwang et al.

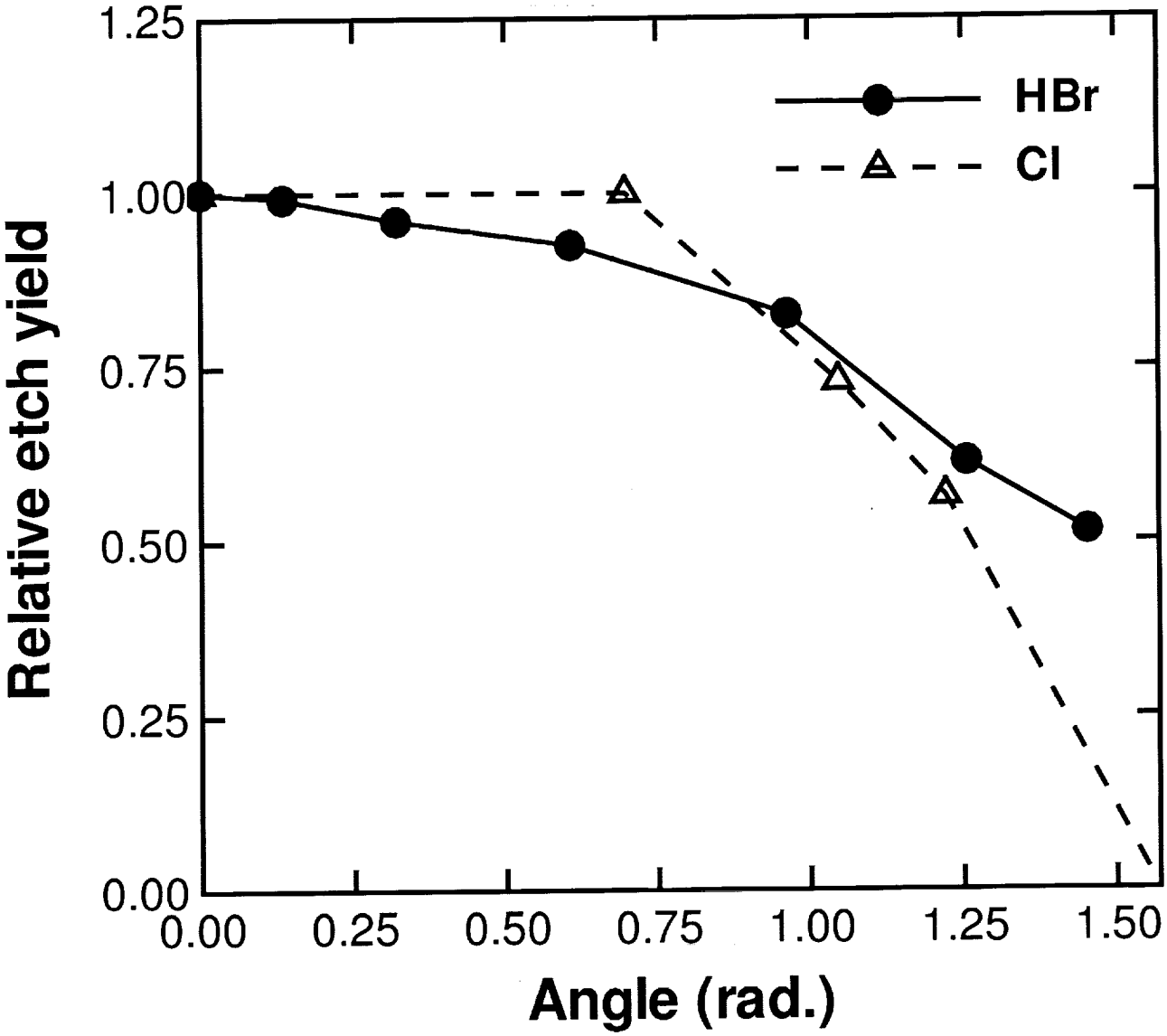

Fig. 9 of 11
Hwang et al.

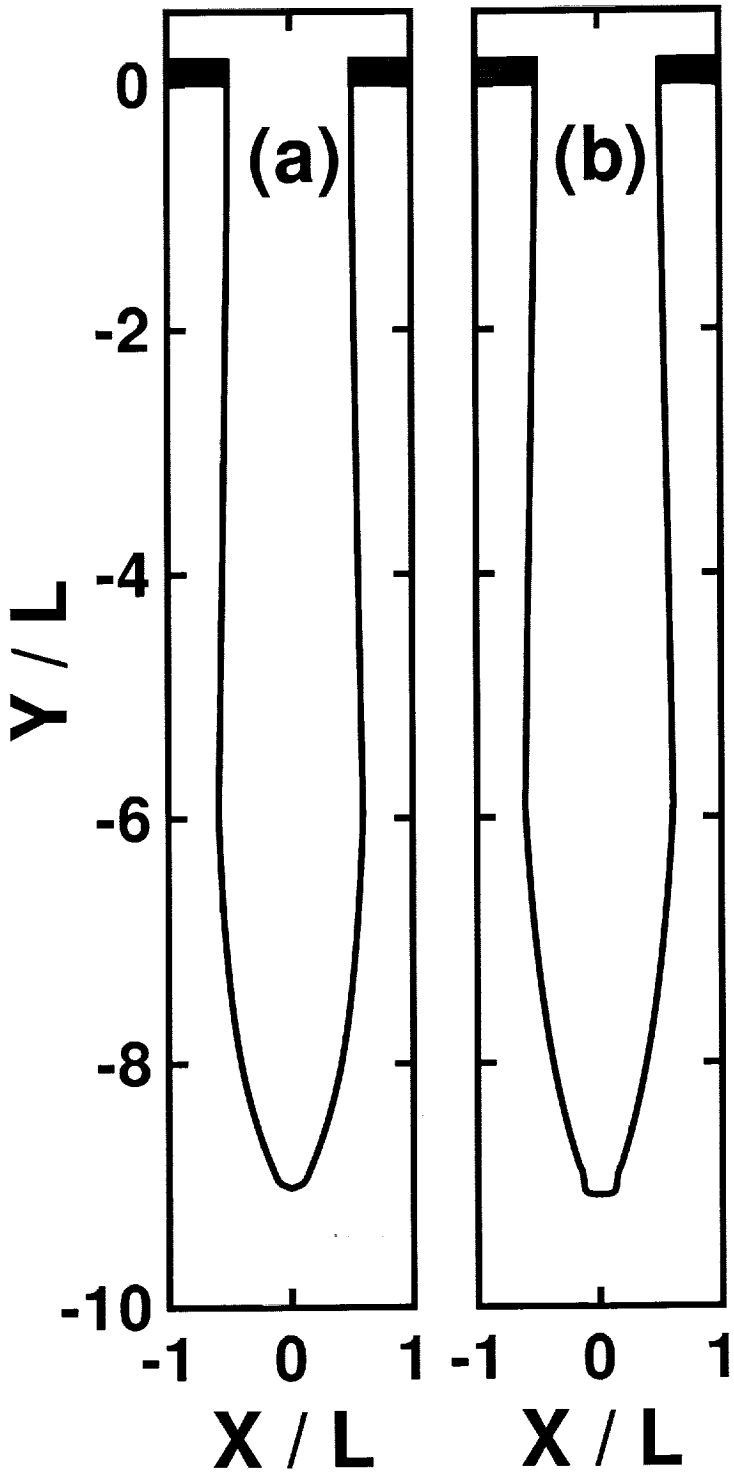

Fig. 10 of 11
Hwang et al.

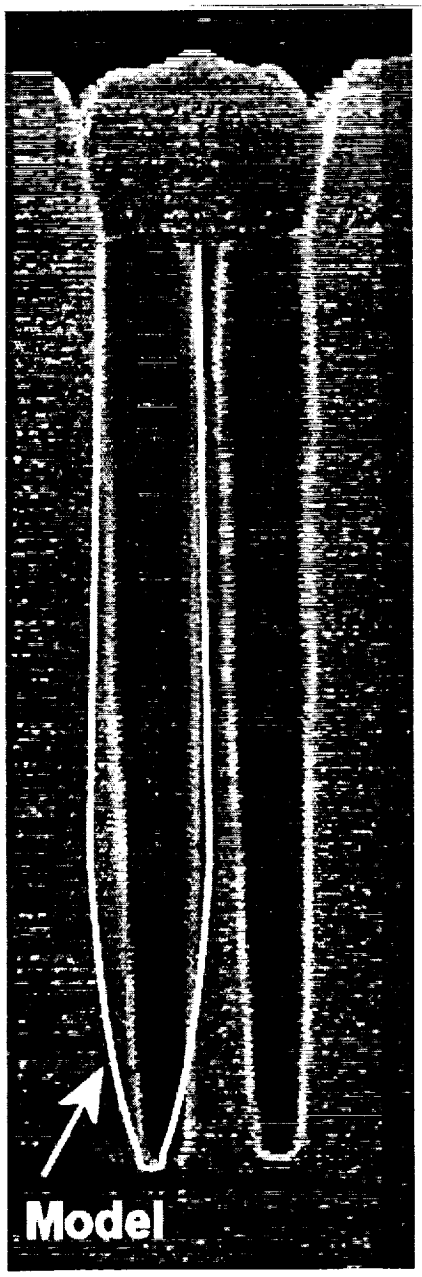

Fig. 11 of 11
Hwang et al.